

ULB, Brussels
Feb 19, 2010

Fitting spectrum and composition of Ultra-High Energy Cosmic Rays

Oleg Kalashev* (INR RAS)

* e-mail: kalashev@ms2.inr.ac.ru

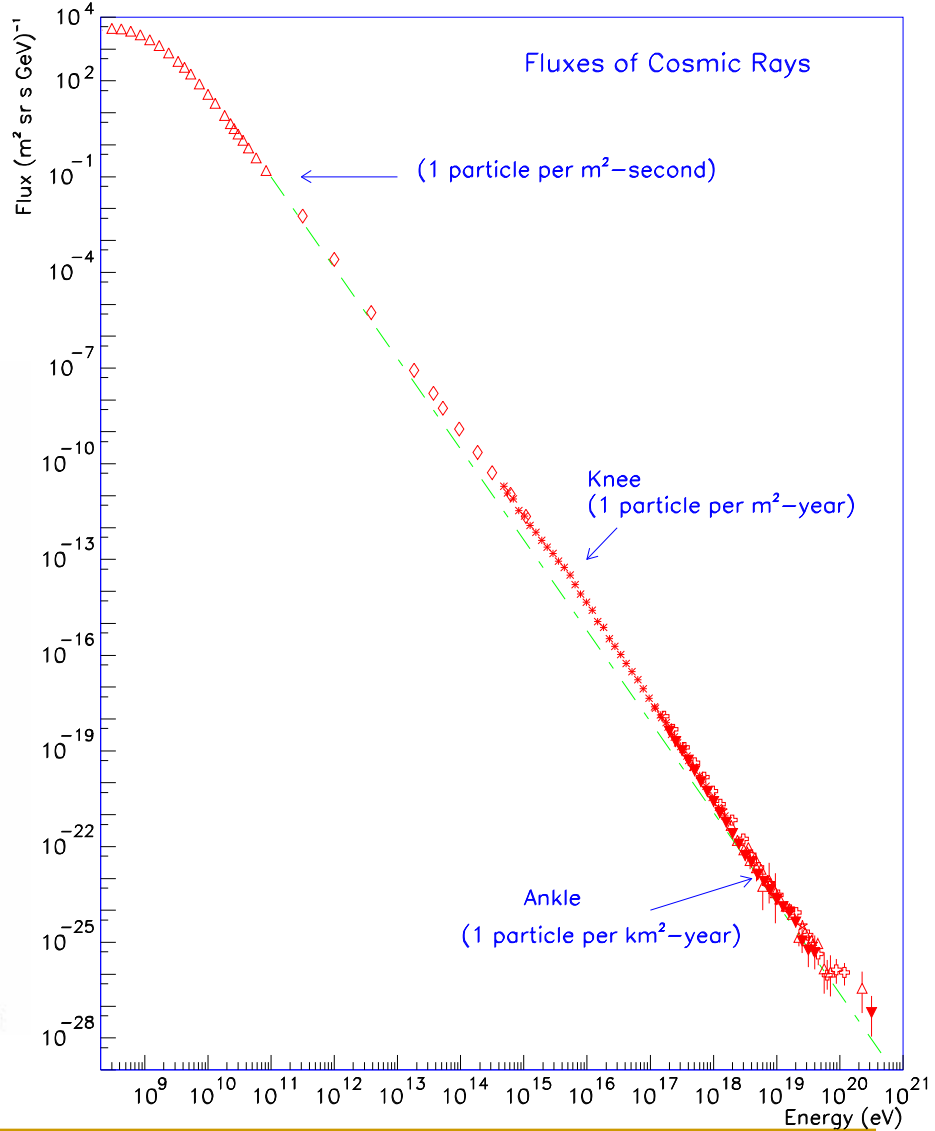
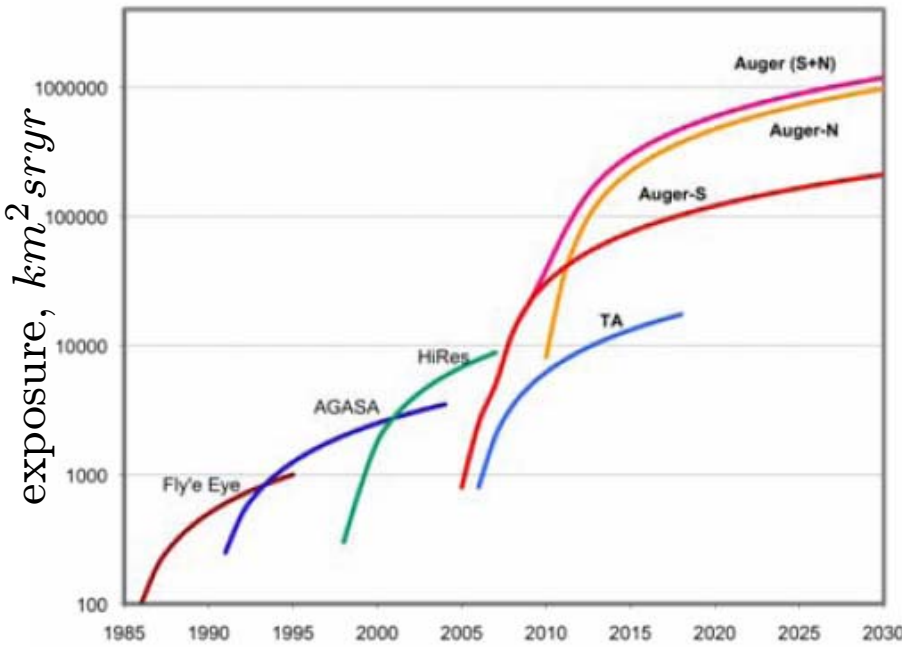
Fitting spectrum and composition of Ultra-High Energy Cosmic Rays

Overview

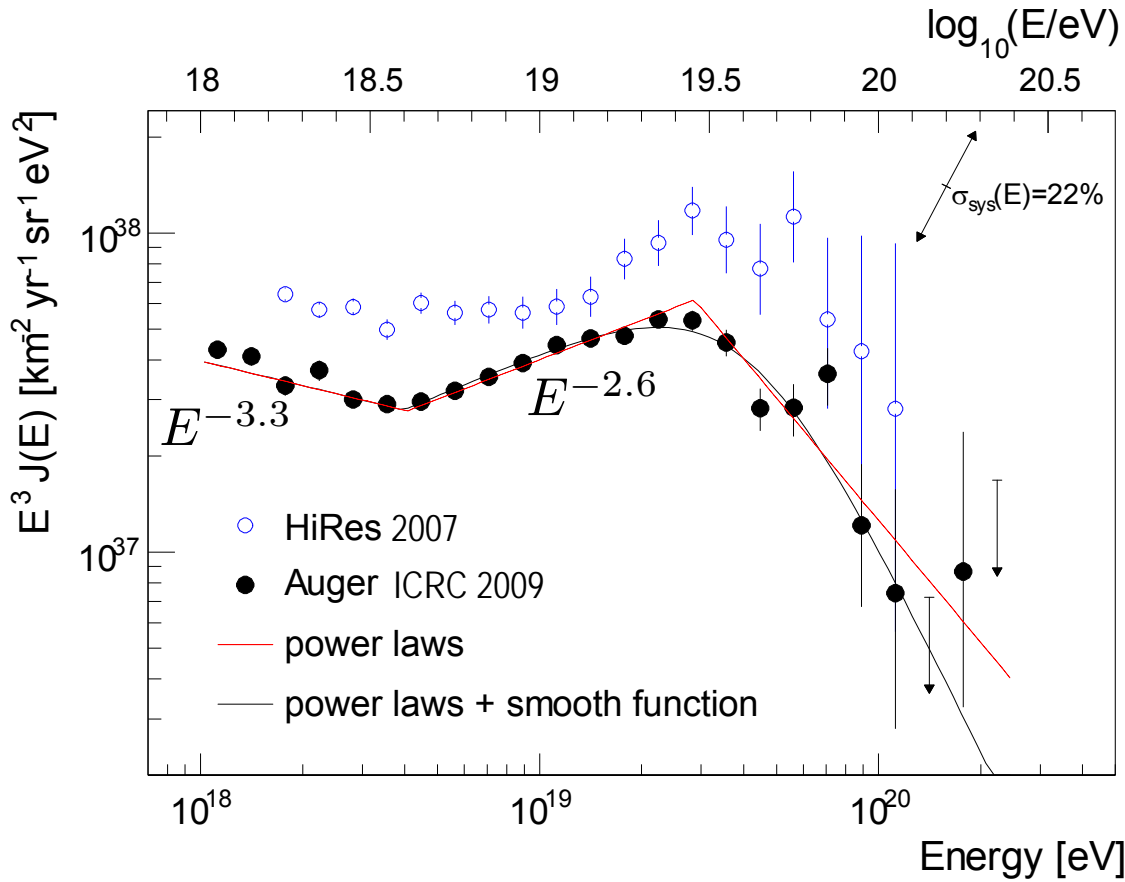
- Introduction
- Propagation of Ultra High Energy Cosmic Rays (UHECR)
 - Main factors
 - Interactions
 - Simulations of cosmic rays propagation
- Fitting experimental spectra and composition
- Conclusion

Observed spectrum of cosmic rays

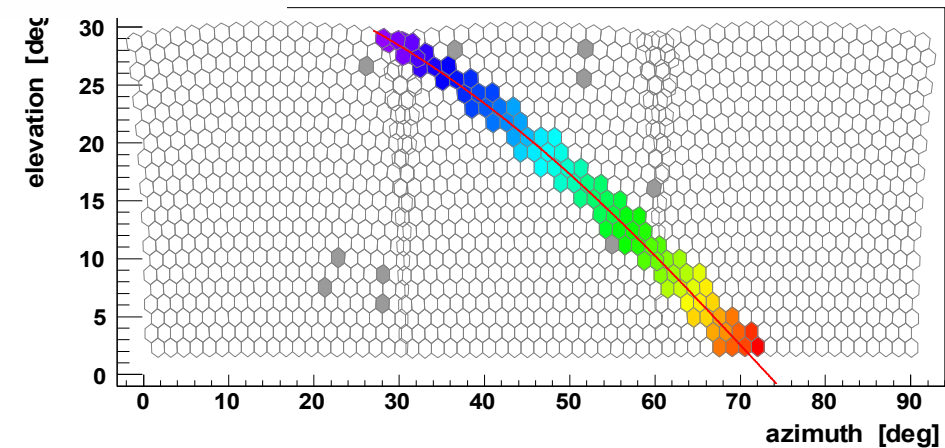
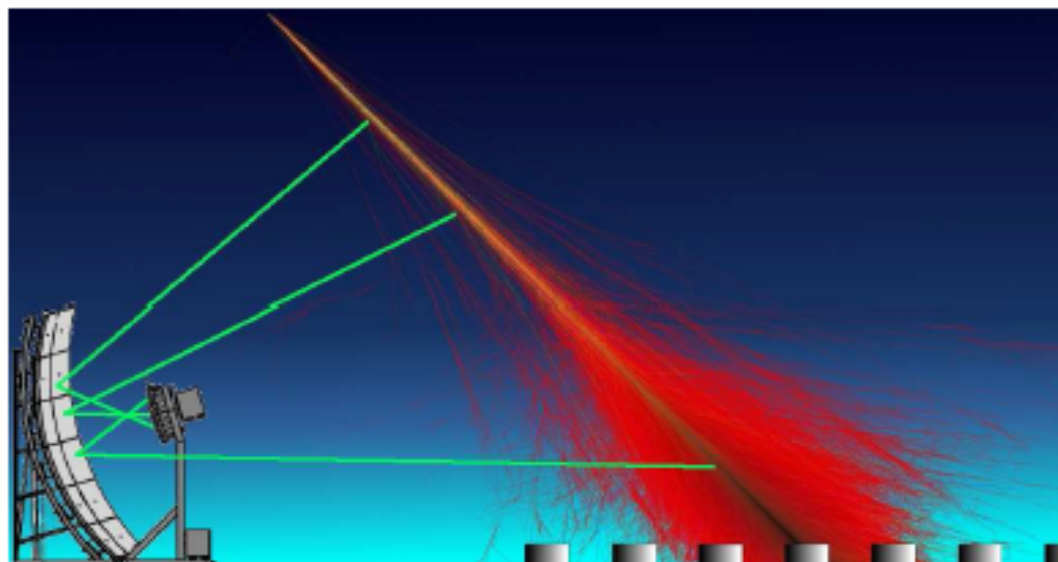
UHECR: $E > 10^{18} eV$



Observed spectrum of cosmic rays



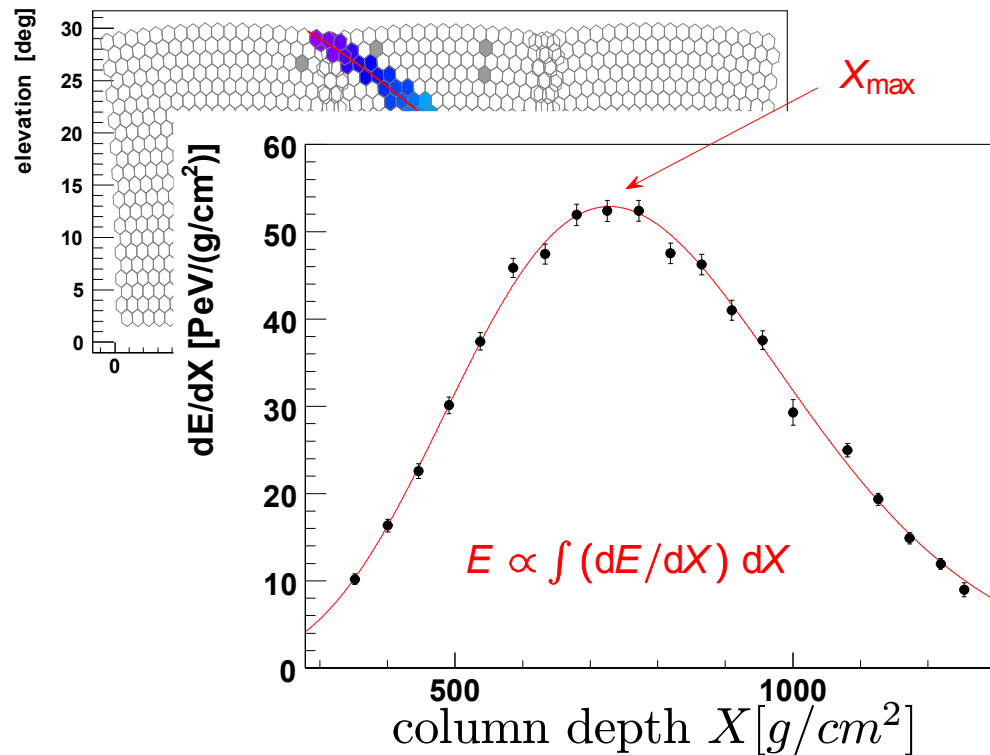
Fluorescence Detector: Longitudinal Shower Profiles



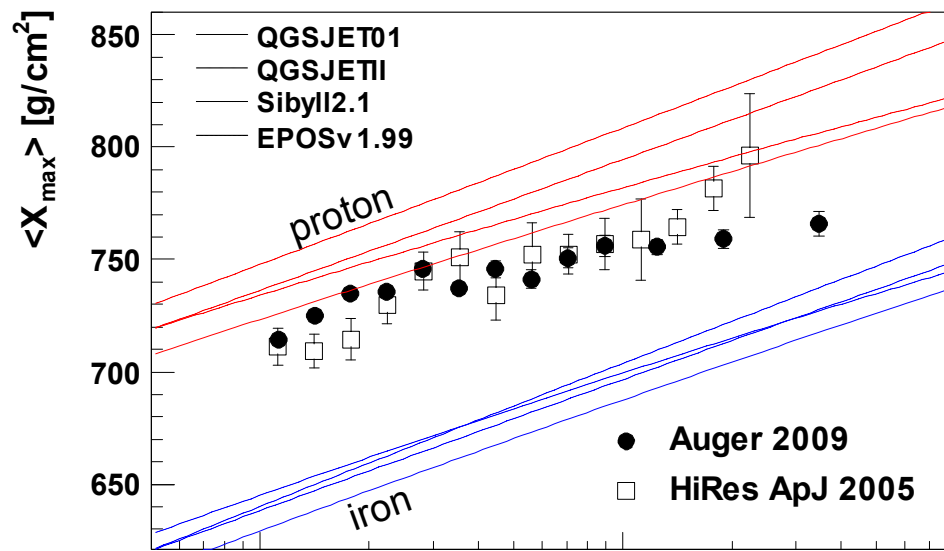
Fitting spectrum and composition of Ultra-High Energy Cosmic Rays

Fluorescence Detector: Longitudinal Shower Profiles

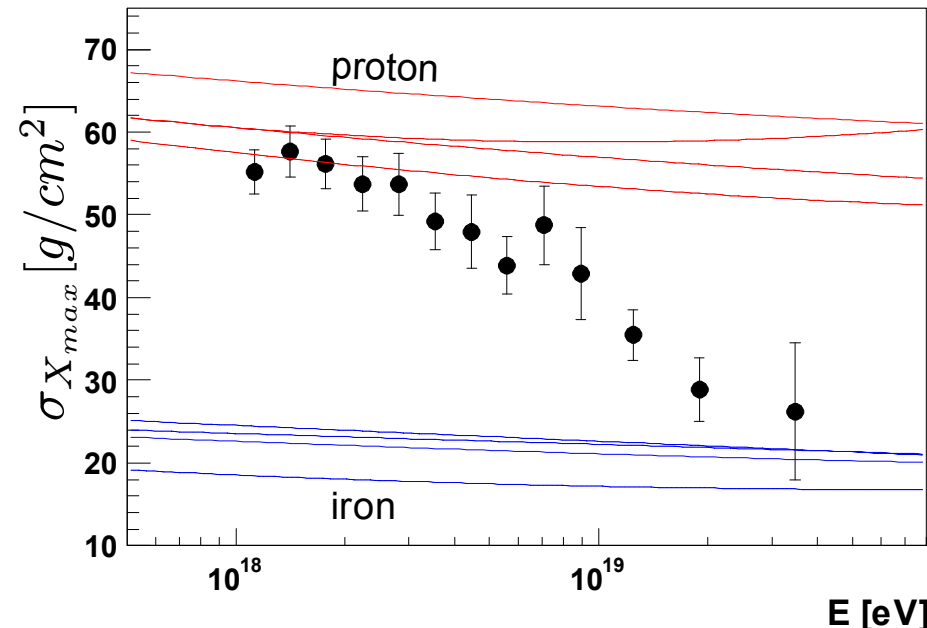
event 1542115, CO



Average Shower Maximum $\langle X_{\max} \rangle$ and RMS(X_{\max})

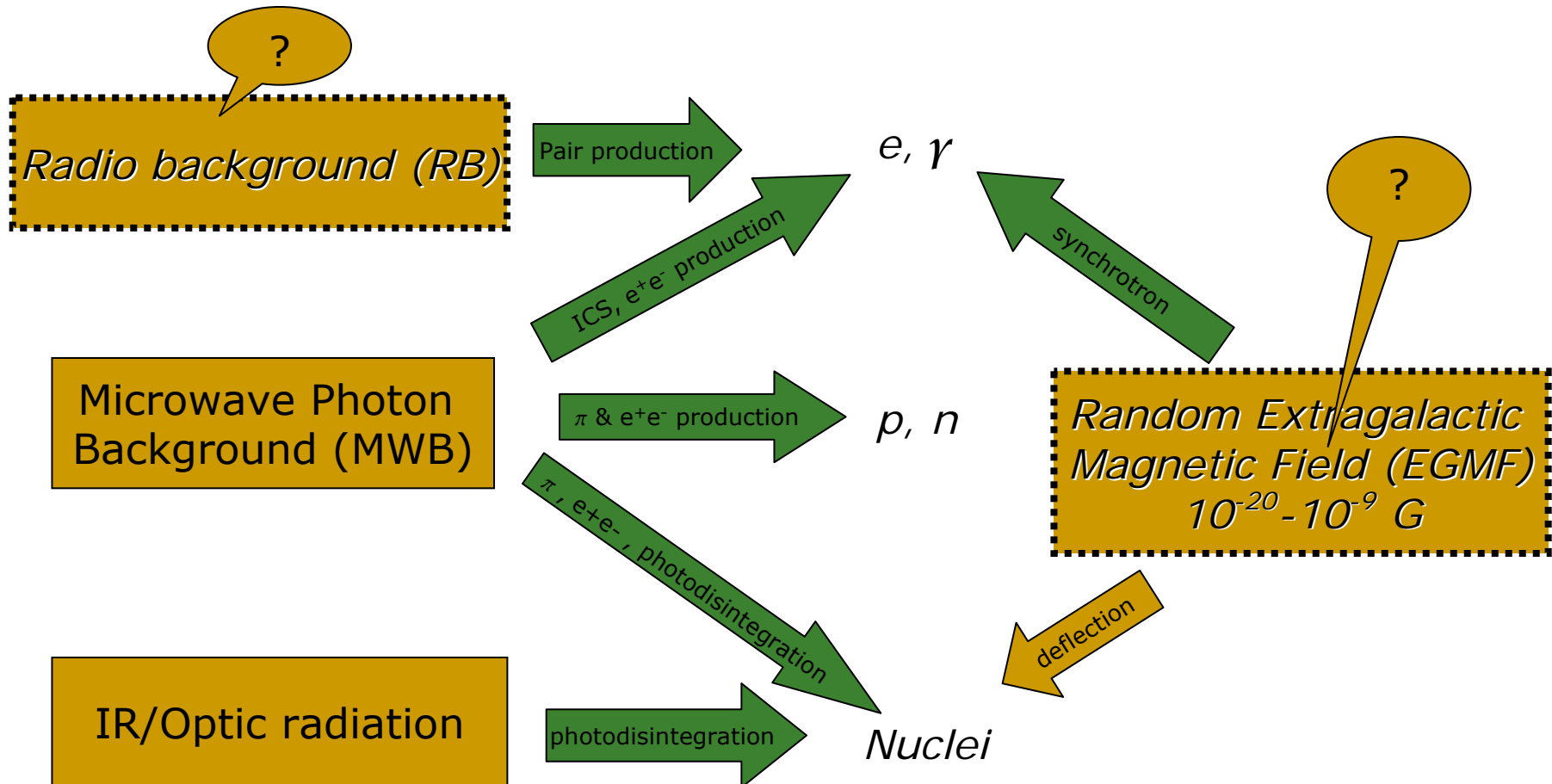


$$\langle X_{\max} \rangle \simeq D \log(E/A) + \text{const}$$



$$\sigma_{X_{\max}}(A_2) < \sigma_{X_{\max}}(A_1) \text{ for } A_2 > A_1$$

Main Factors influencing UHECR propagation



Interactions

■ Protons and neutrons

Pion production

$$N \gamma_b \rightarrow N' \pi \dots$$

e⁺e⁻ pair production

$$p \gamma_b \rightarrow p e^+ e^-$$

neutron β-decay

$$n \rightarrow p e^- \bar{\nu}_e$$

Interactions

■ Protons and neutrons

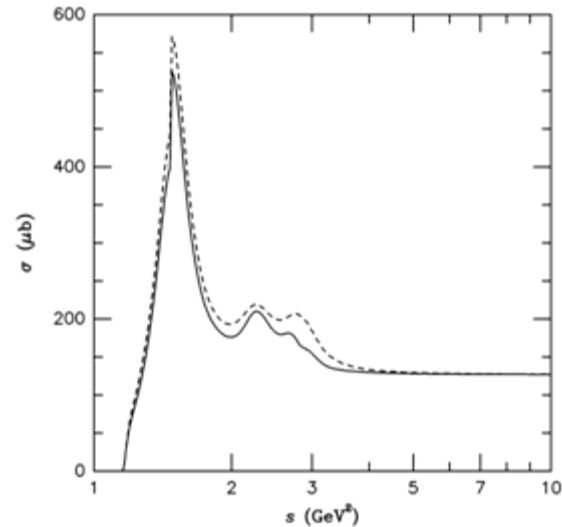
Pion production $N \gamma_b \rightarrow N' \pi \dots$

$$E_{th} = \frac{m_\pi(m_p + m_\pi/2)}{\epsilon} \simeq 7 \times 10^{16} \left(\frac{\epsilon}{eV}\right)^{-1} eV$$

For MWB ($\epsilon \simeq 10^{-3} eV$): $E_{th} \simeq 70 E eV$

e⁺e⁻ pair production $p \gamma_b \rightarrow p e^+ e^-$

neutron β-decay $n \rightarrow p e^- \bar{\nu}_e$



Interactions

■ Protons and neutrons

Pion production $N \gamma_b \rightarrow N' \pi \dots$

$$E_{th} = \frac{m_\pi(m_p + m_\pi/2)}{\epsilon} \simeq 7 \times 10^{16} \left(\frac{\epsilon}{eV} \right)^{-1} eV \quad (1)$$

For MWB ($\epsilon \simeq 10^{-3} eV$): $E_{th} \simeq 70 E eV$

e⁺e⁻ pair production $p \gamma_b \rightarrow p e^+ e^-$

$$E_{th} = \frac{m_e(m_A + m_e)}{\epsilon} \simeq 5 \times 10^{14} \left(\frac{\epsilon}{eV} \right)^{-1} eV \quad (2)$$

For MWB ($\epsilon \simeq 10^{-3} eV$): $E_{th} \simeq 5 \times 10^{17} eV$

neutron β-decay $n \rightarrow p e^- \bar{\nu}_e$

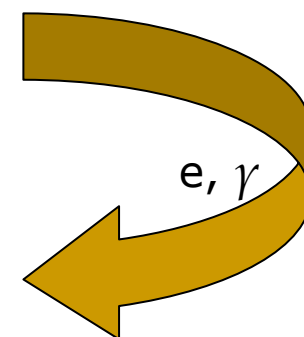
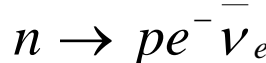
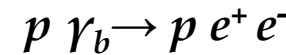
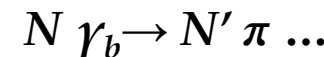
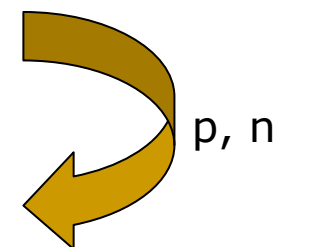
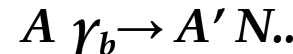
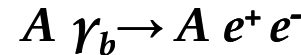
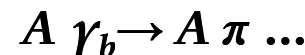
Interactions

■ Nuclei

Pion production

$e^+ e^-$ pair production

Photo-disintegration



■ Protons and neutrons

Pion production

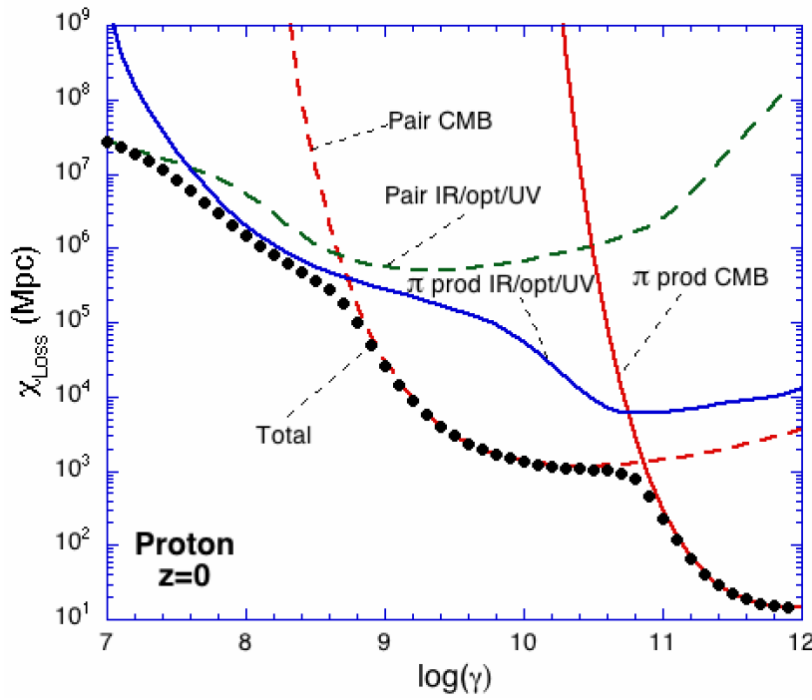
$e^+ e^-$ pair production

neutron β -decay

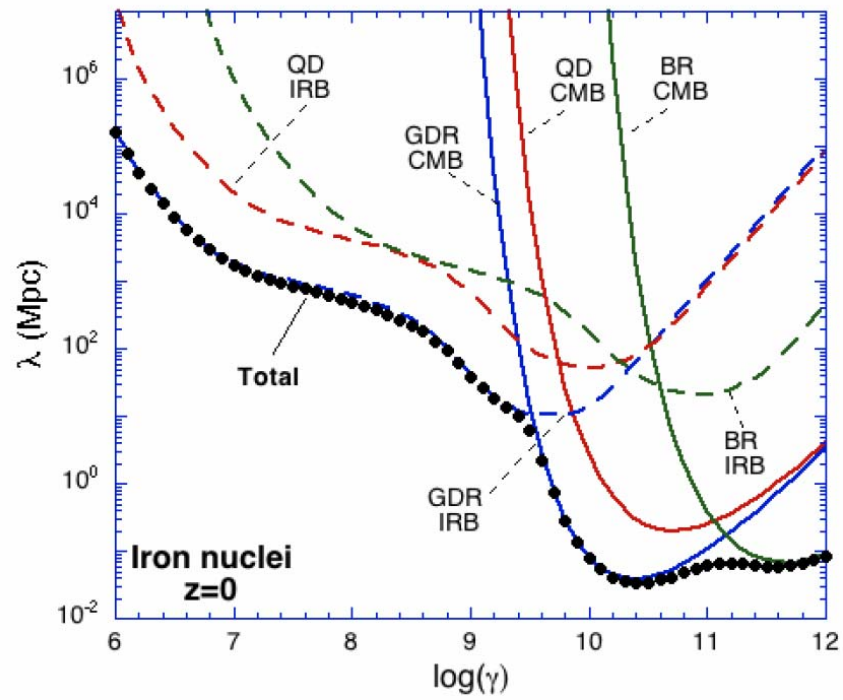
■ Electron-photon cascade

Energy loss lengths

■ Proton



■ Iron



Interactions

■ Protons ,neutrons and nuclei

Pion production

$$A \gamma_b \rightarrow A \pi \dots$$

$e^+ e^-$ pair production

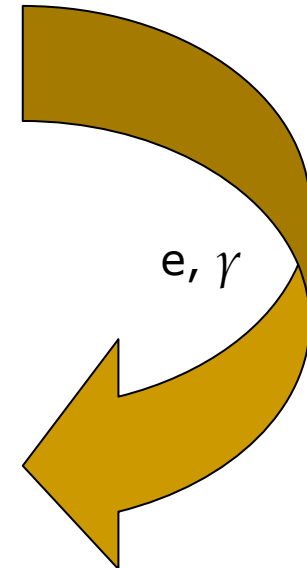
$$A \gamma_b \rightarrow A e^+ e^-$$

Photo-disintegration

$$A \gamma_b \rightarrow A' N..$$

neutron β -decay

$$n \rightarrow p e^- \bar{\nu}_e$$



■ Electron-photon cascade

Inverse Compton

$$e \gamma_b \rightarrow e \gamma$$

$e^+ e^-$ pair production

$$\gamma \gamma_b \rightarrow e^+ e^-$$

$$E_{th} = \frac{m_e^2}{\epsilon} \simeq 2.6 \times 10^{11} \left(\frac{\epsilon}{eV} \right)^{-1} eV$$

For MWB ($\epsilon \simeq 10^{-3} eV$): $E_{th} \simeq 5 \times 10^{14} eV$

Interactions

■ Protons ,neutrons and nuclei

Pion production

$$A \gamma_b \rightarrow A \pi \dots$$

$e^+ e^-$ pair production

$$A \gamma_b \rightarrow A e^+ e^-$$

Photo-disintegration

$$A \gamma_b \rightarrow A' N..$$

neutron β -decay

$$n \rightarrow p e^- \bar{\nu}_e$$

■ Electron-photon cascade

Inverse Compton

$$e \gamma_b \rightarrow e \gamma$$

$e^+ e^-$ pair production

$$\gamma \gamma_b \rightarrow e^+ e^-$$

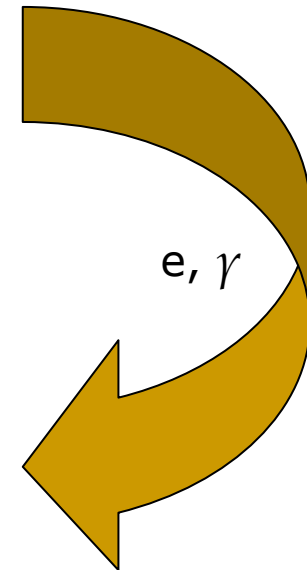
Synchrotron losses

Double pair production

$$\gamma \gamma_b \rightarrow e^+ e^- e^+ e^-$$

$e^+ e^-$ pair production by e

$$e \gamma_b \rightarrow e e^+ e^-$$



Interactions

■ Electron-photon cascade

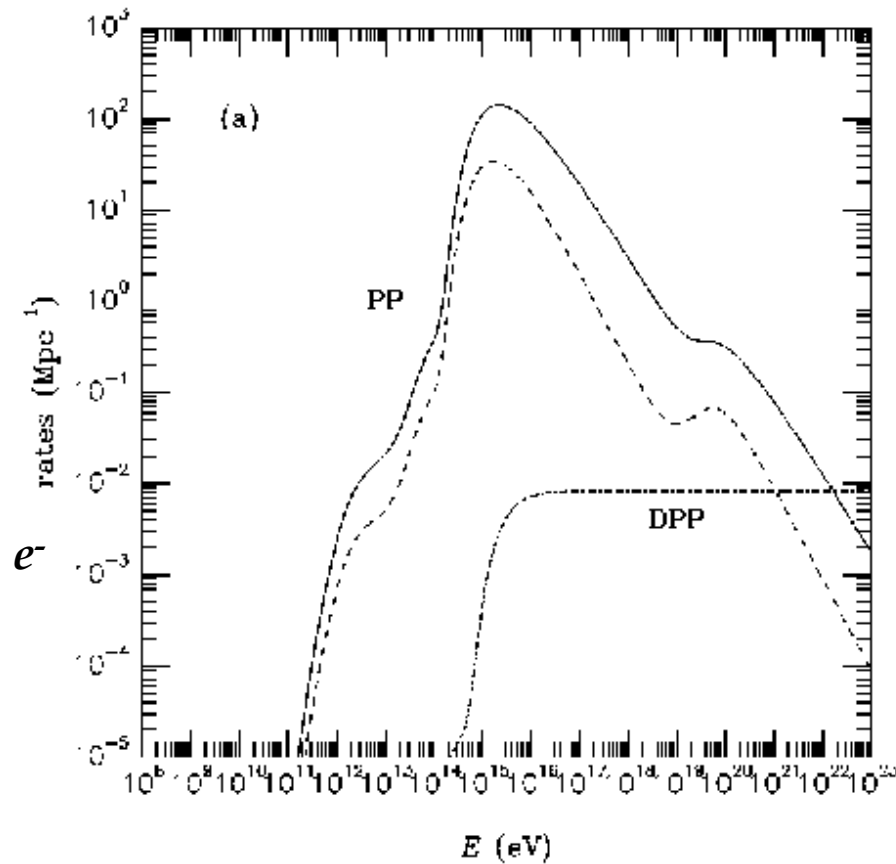
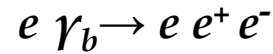
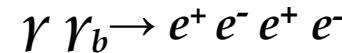
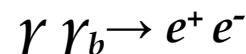
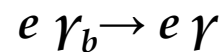
Inverse Compton

$e^+ e^-$ pair production

Synchrotron losses

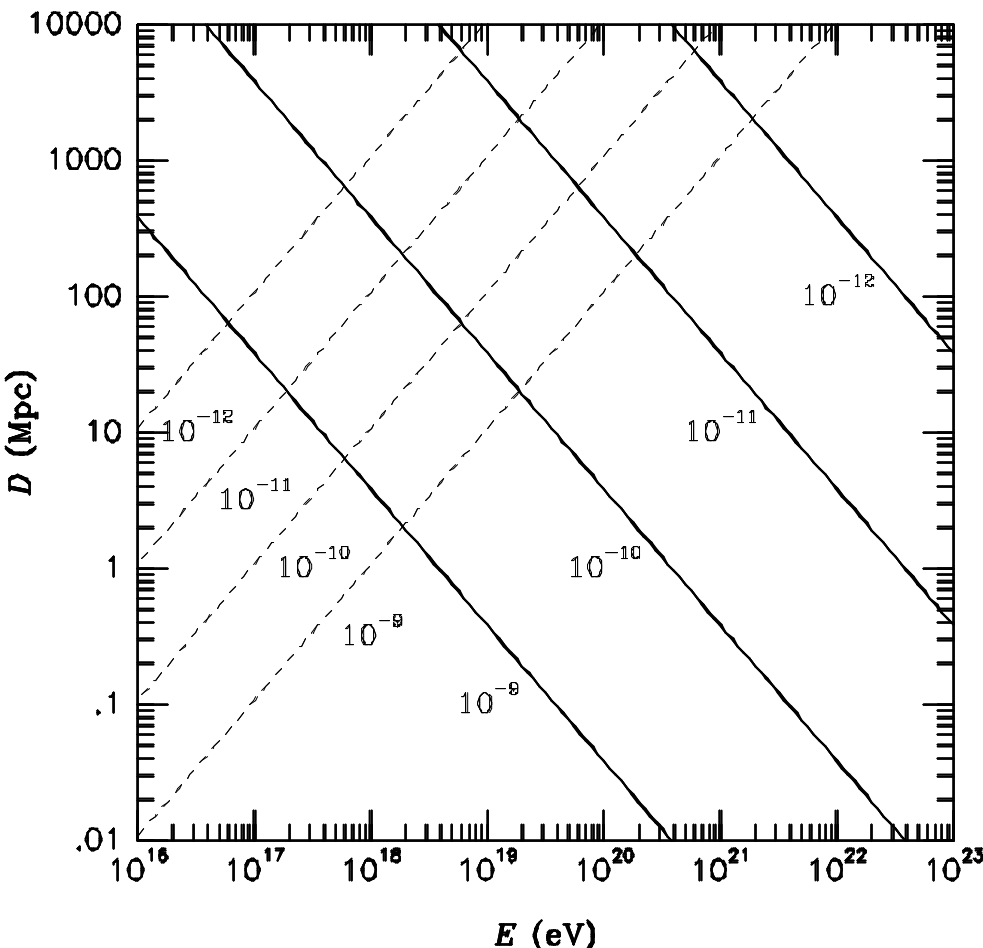
Double pair production

$e^+ e^-$ pair production by e



Deflection and synchrotron radiation

Gyroradius: $R_g = \frac{E}{qeB_\perp} \simeq 110 \times \frac{1}{Z} \left(\frac{E}{10^{19} \text{ eV}} \right) \left(\frac{B_\perp}{10^{-10} \text{ G}} \right)^{-1} \text{ Mpc}$



Synchrotron loss length:

$$\frac{dE}{dt} = -\frac{4}{3}\sigma_T \frac{B^2}{8\pi} \left(\frac{qm_e}{m} \right)^4 \left(\frac{E}{m_e} \right)^2$$

$$E_\gamma \simeq \frac{3eB}{2m_e} \left(\frac{E_e}{m_e} \right)^2 \simeq$$

$$2.2 \times 10^{14} \left(\frac{E_e}{10^{21} \text{ eV}} \right)^2 \left(\frac{B}{10^{-9} \text{ G}} \right) \text{ eV}$$

The gyroradius and the synchrotron loss rates of electrons for various strengths of the EGMF

Some references on UHECR propagation

π production

A.Mucke et al., Comp.Phys.Comm.124,290(2000)

Photodisintegration

F.Stecker et al. Astrophys.J. 512 (1999) 521-526.
E.Khan et al. Astropart.Phys. 23 (2005) 191-201

e⁺e⁻ pair production

M.J.Chodorowski et al. Astrophys.J.400,181(1992)

Extragalactic magnetic field

K.Dolag et al., astro-ph/0410419

Infrared background

F.Stecker et al. astro-ph/0510449

Radio background

T.A. Clark, L.W. Brown, and J.K. Alexander, Nature 228, 847
R.J. Protheroe, P.L. Biermann, Astropart. Phys. 6, 45

Simulations of cosmic rays propagation

- Monte Carlo based simulations
 - Random extragalactic magnetic field is taken into account
- Transport equation approach (rectilinear propagation)
 - Fast calculation (good for parameter space scanning)
 - Gives correct result for

$$E \geq 10^{17} eV \times Z \times \frac{B}{10^{-10} G}, \quad L_{cor} = 1 Mpc$$

or for homogeneous source distribution if distance to the closest source is less than diffuse length

Simulations of cosmic rays propagation

Sample transport equation for electrons (includes only pair production PP and inverse Compton scattering ICS)

$$\begin{aligned} \frac{d}{dt}N_e(E_e, t) = & -N_e(E_e, t) \int d\epsilon n(\epsilon) \int d\mu \frac{1 - \beta_e \mu}{2} \sigma_{\text{ICS}}(E_e, \epsilon, \mu) + \\ & \int dE'_e N_e(E'_e, t) \int d\epsilon n(\epsilon) \int d\mu \frac{1 - \beta'_e \mu}{2} \frac{d\sigma_{\text{ICS}}}{dE_e}(E_e; E'_e, \epsilon, \mu) + \\ & \int dE_\gamma N_\gamma(E_\gamma, t) \int d\epsilon n(\epsilon) \int d\mu \frac{1 - \mu}{2} \frac{d\sigma_{\text{PP}}}{dE_e}(E_e; E_\gamma, \epsilon, \mu) + Q(E_e, t) \end{aligned}$$

Fitting experimental data

- Energy spectrum $j(E)$
- Chemical composition
 - Average Shower Maximum $\langle X_{\max} \rangle (E)$
 - Shower-to-Shower Fluctuations $\sigma(X_{\max}) (E)$

Fitting experimental data

■ Energy spectrum $j(E)$

- Binned maximum likelihood function is used
- Poisson probability of the observed event set is maximized

$$L(\mathbf{n}; \boldsymbol{\nu}) = \prod_i^N \frac{\nu_i^{n_i}}{n_i!} e^{\nu_i}$$

- Goodness of fit defined as fraction of hypothetical experiments which result in worse agreement with the theory than the real data having the same total number of events

Phenomenological source model:

$$F(E, z) = f E^{-\alpha} \text{Exp}(-E/E_{max}) (1+z)^{3+m} \Theta(z-z_{min}) \Theta(z_{max}-z)$$

z – red shift, $\Theta(x)$ -step function

Phenomenological source model:

$$F(E, z) = f E^{-\alpha} \text{Exp}(-E/E_{max}) (1+z)^{3+m} \Theta(z-z_{min}) \Theta(z_{max}-z)$$

z – red shift, $\Theta(x)$ -step function

Parameter	Name	Typical Values
Power of the Injection Spectrum, $E^{-\alpha}$	α	$1 \leq \alpha \leq 2.7$
End point of the Energy Spectrum	E_{max}	$2 \times 10^{20} \leq E_{max} \leq 10^{21}$
Evolution factor: $(1+z)^{3+m}$	m	$0 \leq m \leq 4$
Red shift of the nearest source	z_{min}	$0 < z_{min} < 0.01$
Maximal source redshift	z_{max}	$3 < z_{max} < 6$

Fitting experimental data

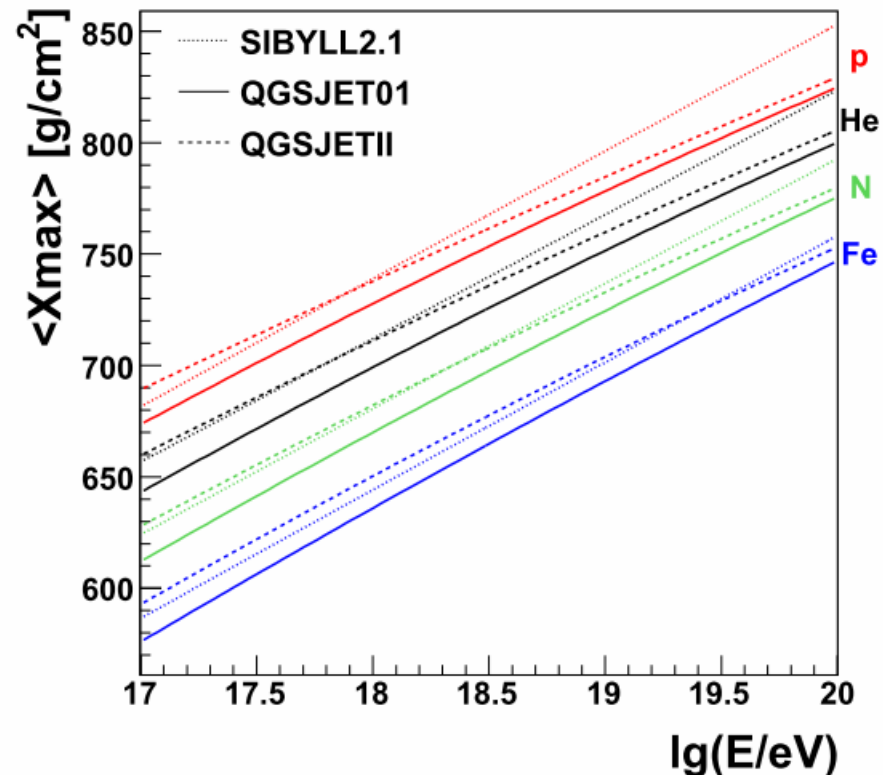
■ Chemical composition

- $\langle X_{max} \rangle (E)$
- $\sigma(X_{max}) (E)$

$$\langle X_{max} \rangle \simeq D \log(E/A) + const$$

For mixed composition:

$$\langle X_{max} \rangle = \sum_A \frac{N_A}{N_{tot}} \langle X_{max} \rangle_A$$



Fitting experimental data

■ Chemical composition

- $\langle X_{max} \rangle (E)$
- $\sigma(X_{max}) (E)$

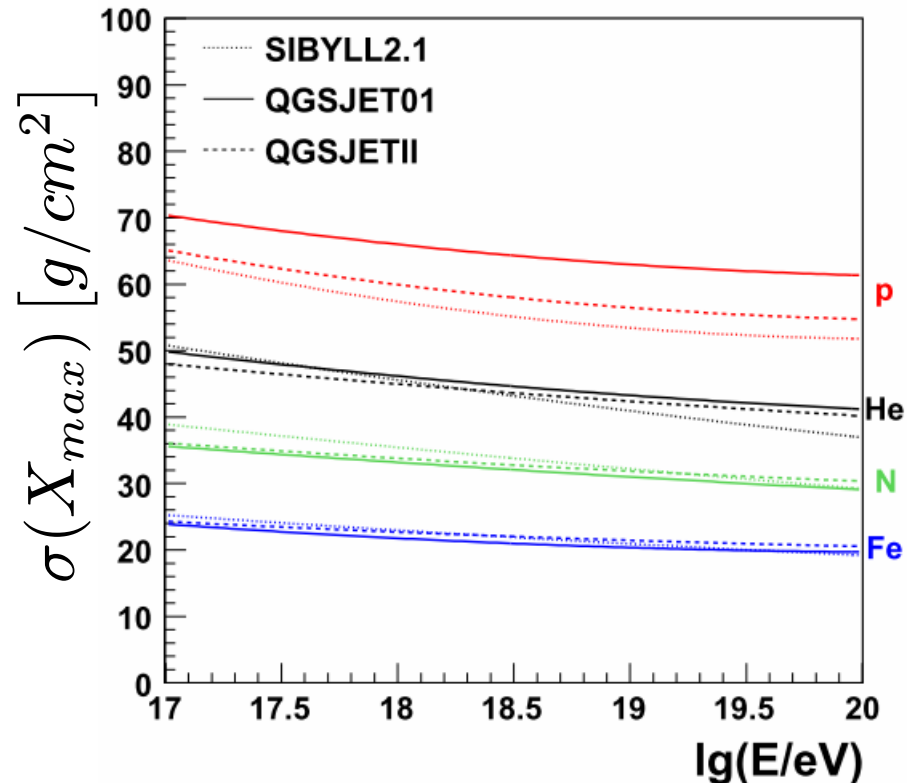
$$\sigma_A(X_{max}) \simeq \sigma_p(X_{max}) A^{-\alpha}$$

$\alpha \simeq 0.2$ for QGSJET01

For mixed composition:

$$RMS(X_{max})^2 = \sum_A \frac{N_A}{N_{tot}} RMS_A(X_{max})^2$$

$$\sigma(X_{max})^2 = RMS(X_{max})^2 - \langle X_{max} \rangle^2$$

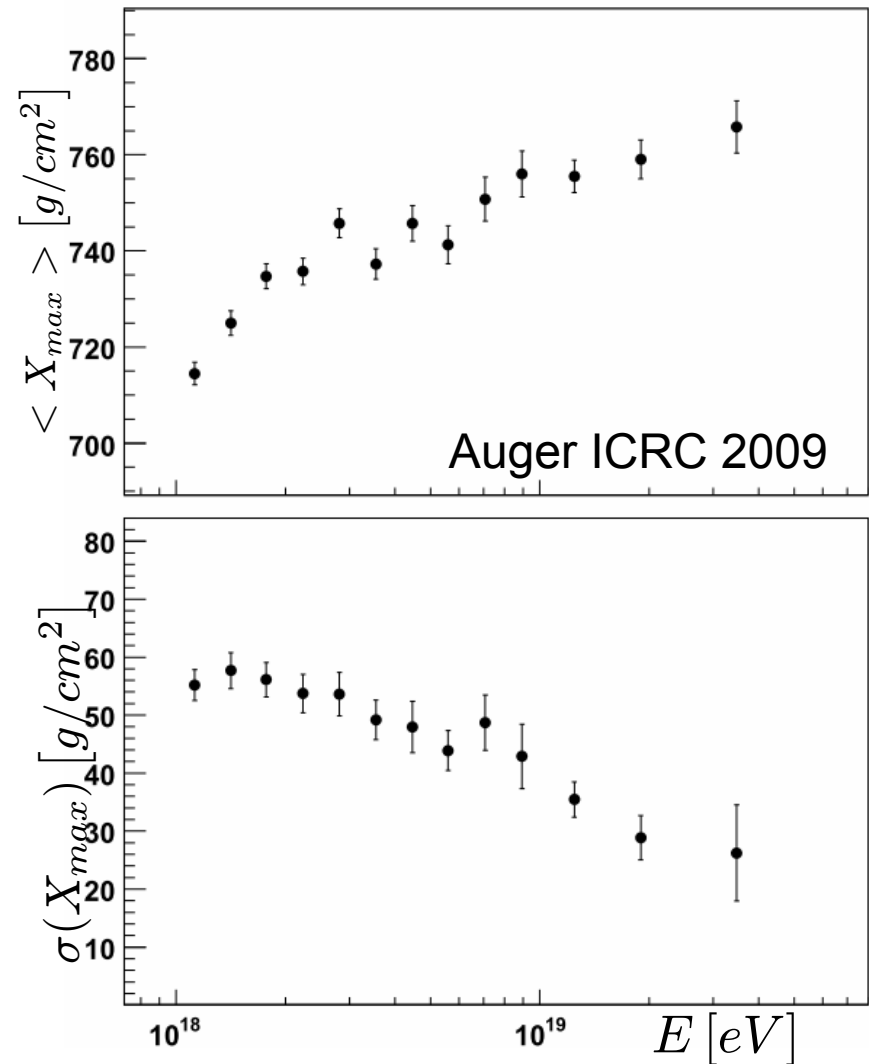


Joint fit of the spectrum and composition

χ^2 statistics is used to obtain goodness of joint fit

Bins with small number of events are combined into larger bins

Goodness of spectrum fit in the bins with small number of events is calculated separately

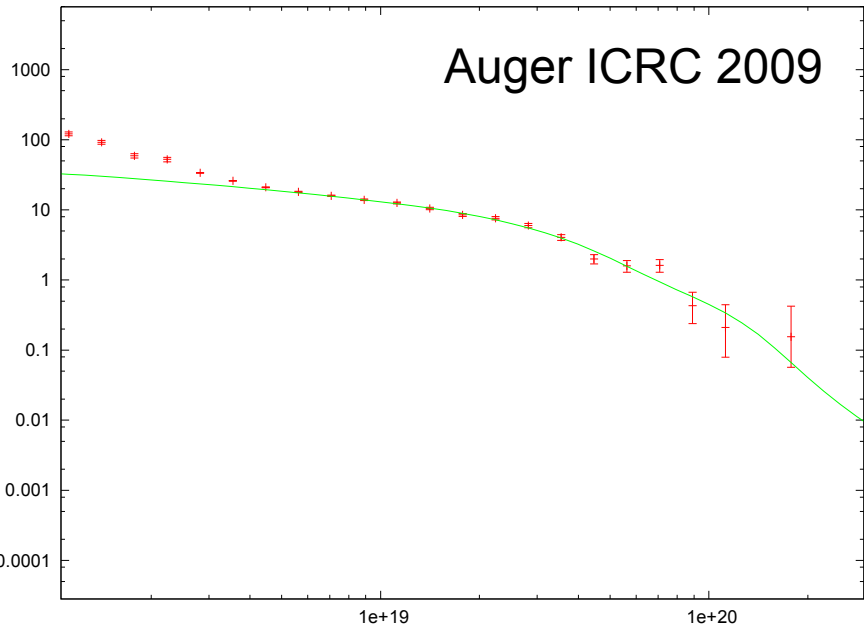


Spectrum and composition fitting examples

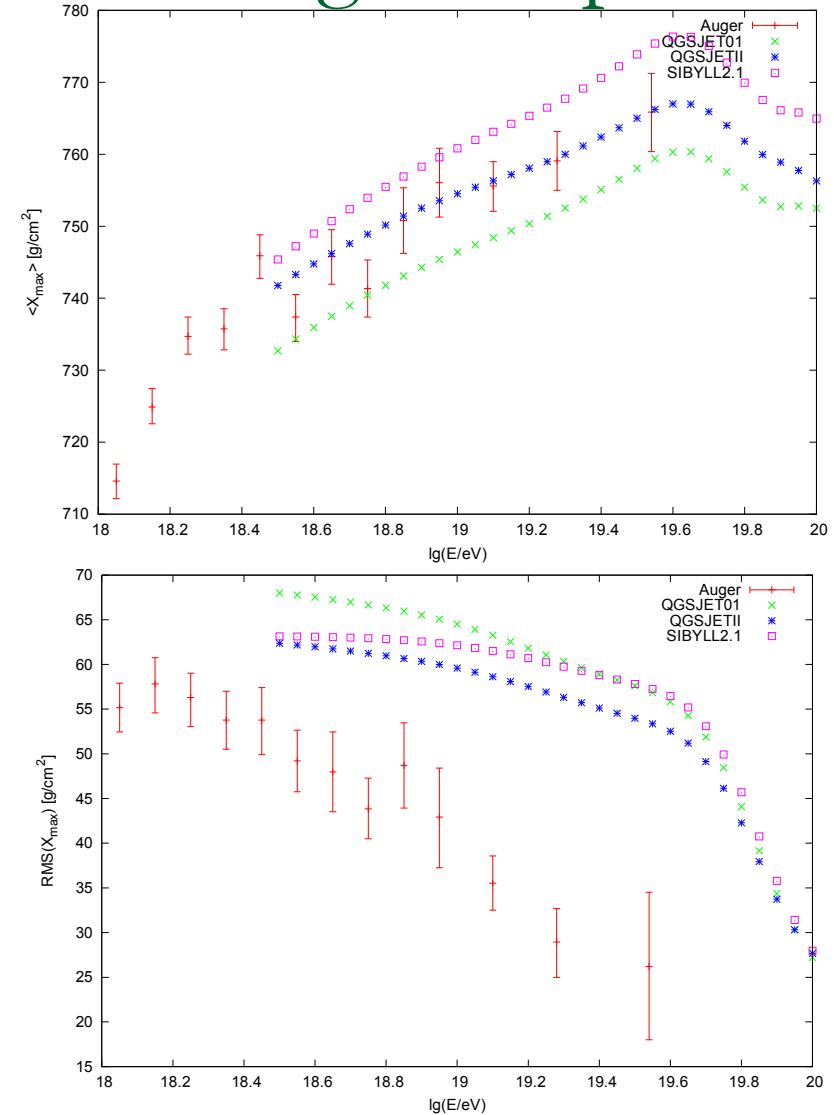
Fe + p $E_{fit} \geq 8EeV$

p:51% Fe:49%

$\alpha = 2; E_{max} = Z25EeV; m = -2$



Spectrum & Xmax fit goodness 0.31

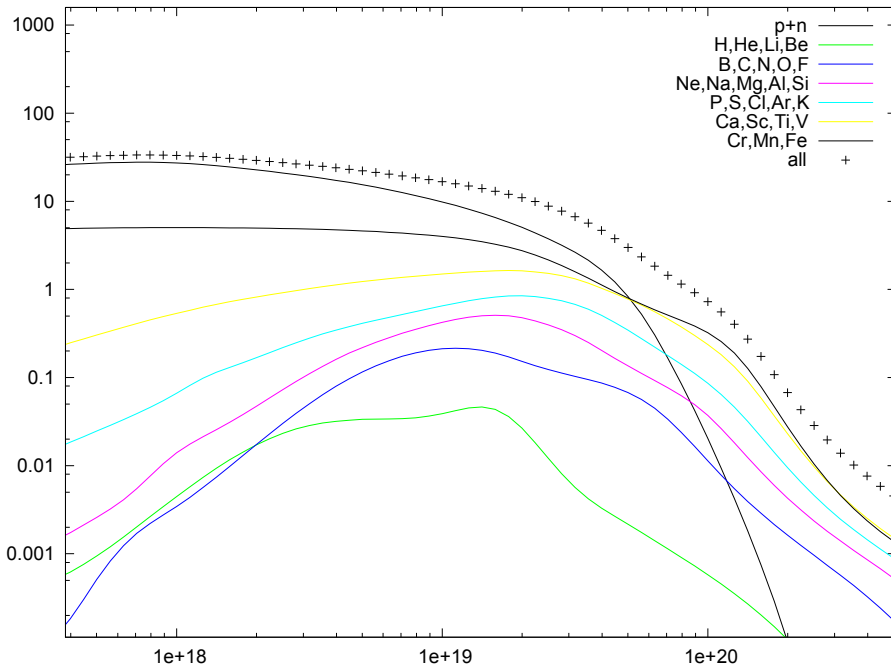


Spectrum and composition fitting examples

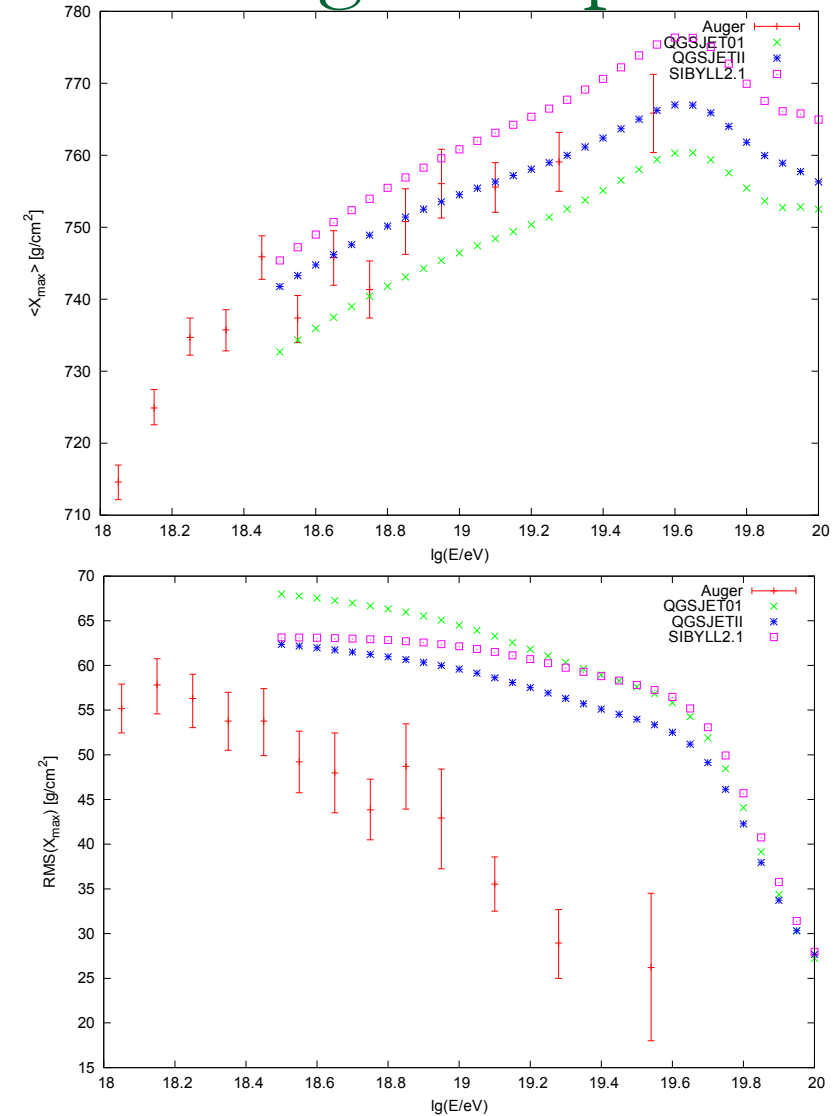
Fe + p $E_{fit} \geq 8EeV$

p:51% Fe:49%

$$\alpha = 2; E_{max} = Z25EeV; m = -2$$



Spectrum & Xmax fit goodness 0.31

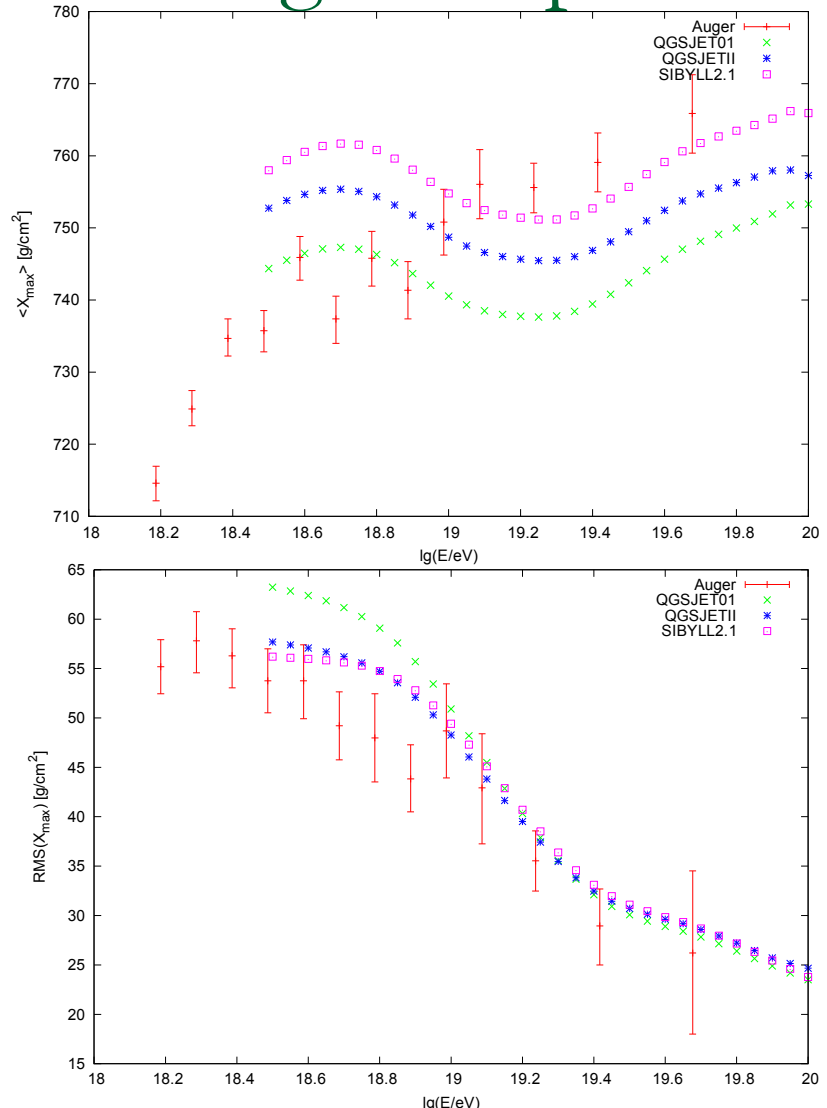
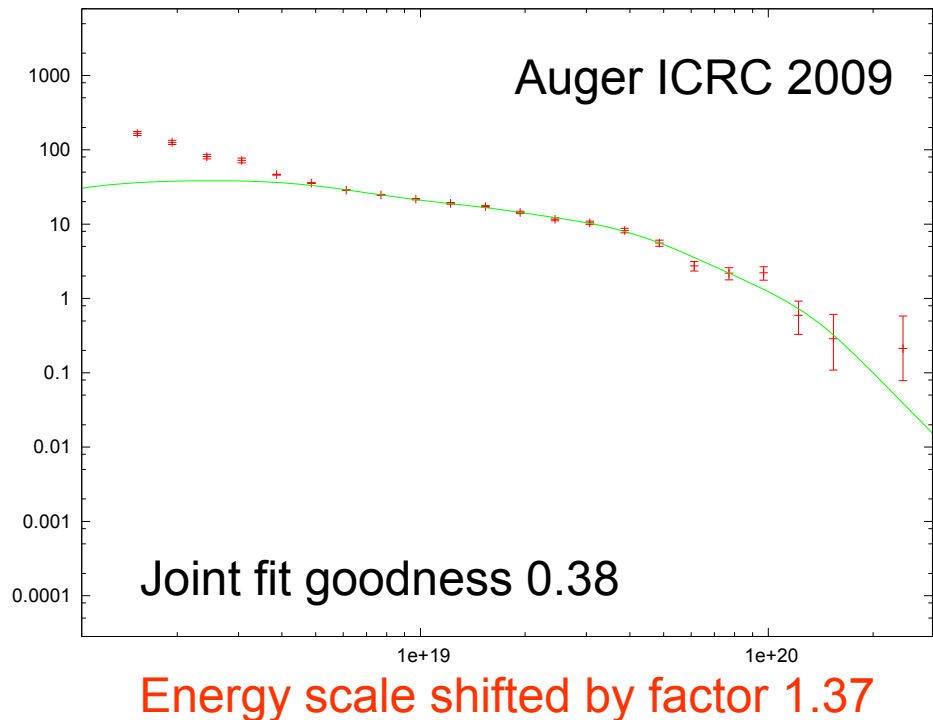


Spectrum and composition fitting examples

Mixed Composition Model (using galactic abundances)

Du Vernois M .A and Thayer, M. R., 1996, ApJ, 465, 982

$$p: 13\% \text{ mixed:} 87\% \quad E_{fit} \geq 8EeV$$
$$\alpha = 0.5; E_{max} = Z4EeV; m = -2$$



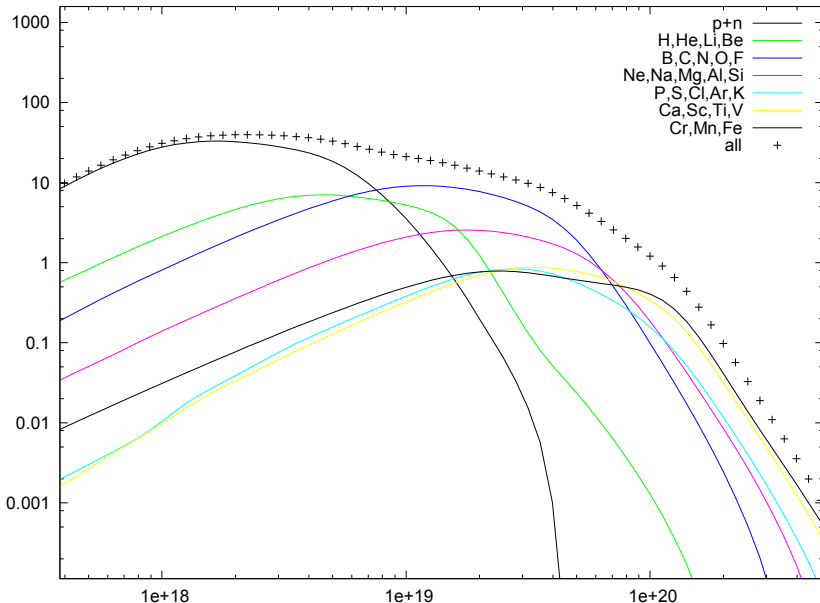
Spectrum and composition fitting examples

Mixed Composition Model (using galactic abundances)

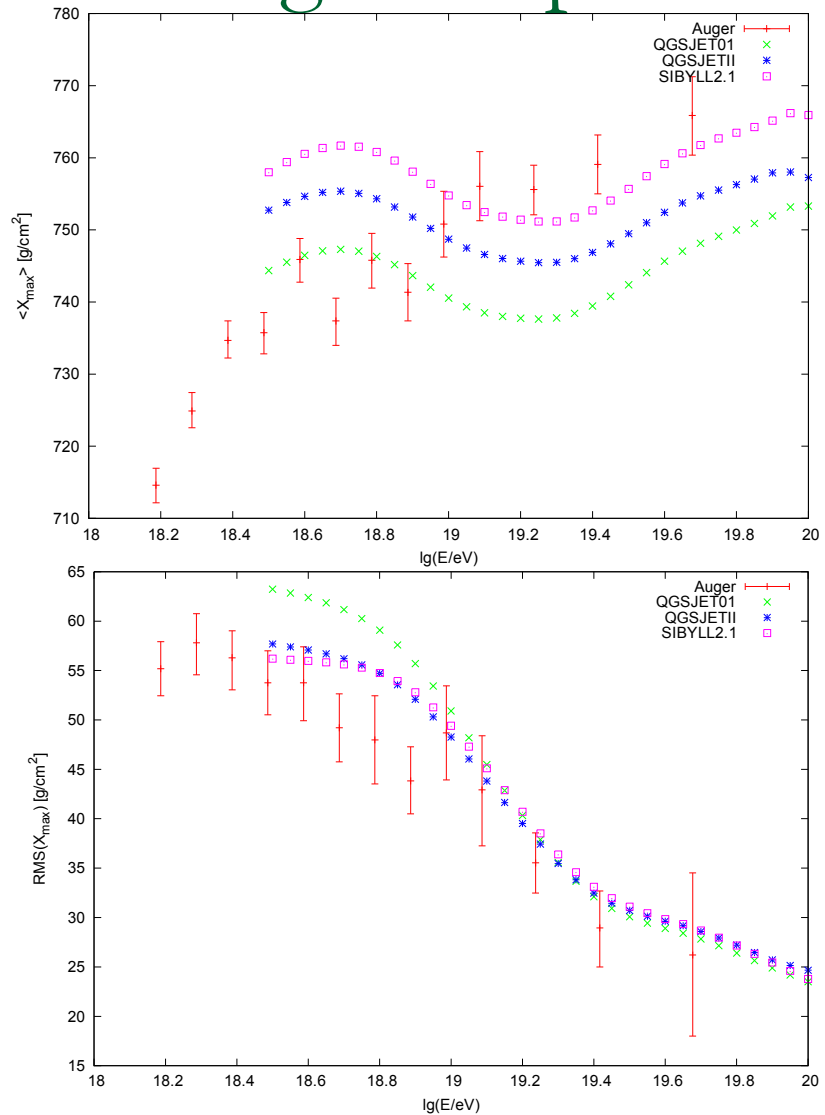
Du Vernois M .A and Thayer, M. R., 1996, ApJ, 465, 982

$$p: 13\% \quad \text{mixed:} 87\% \quad E_{fit} \geq 8EeV$$

$$\alpha = 0.5; E_{max} = Z4EeV; m = -2$$



Energy scale shifted by factor 1.37



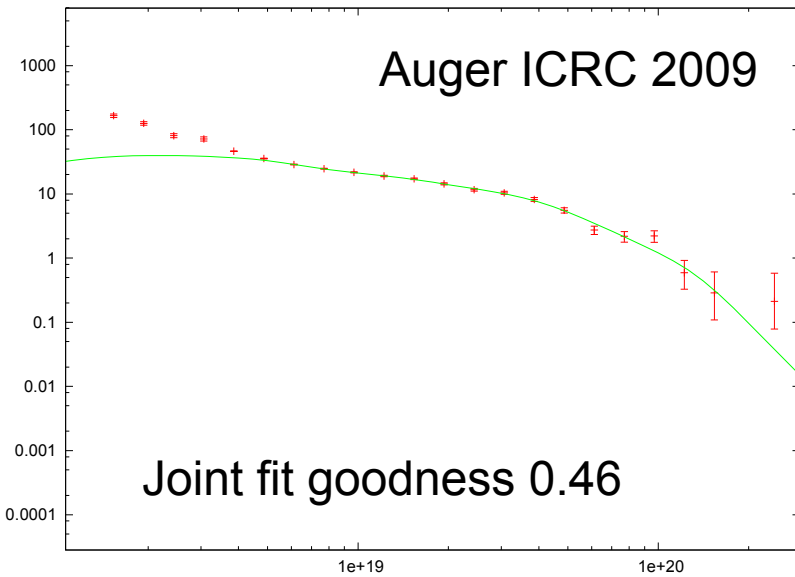
Spectrum and composition fitting examples

mixed + p + He

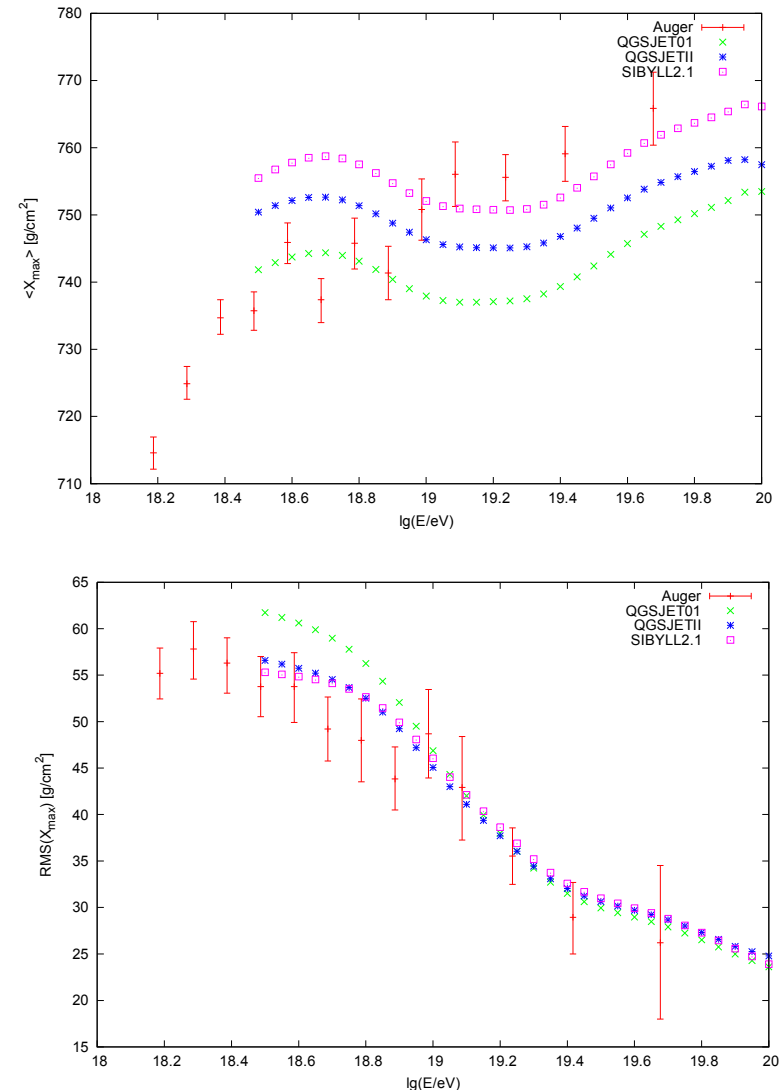
$$E_{fit} \geq 8 EeV$$

p: 4% He: 11% mixed:85%

$$\alpha = 0.5; E_{max} = Z4 EeV; m = -2$$



Energy scale shifted by factor 1.37



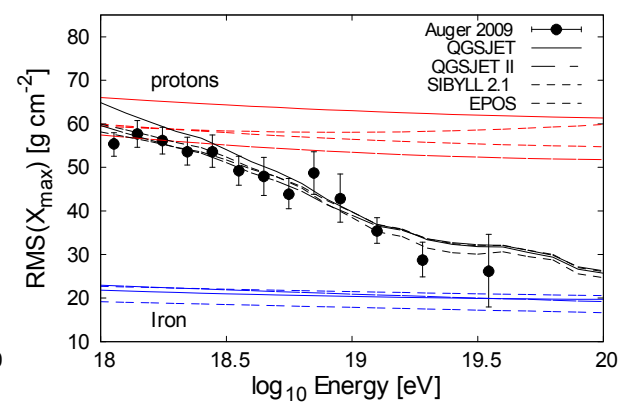
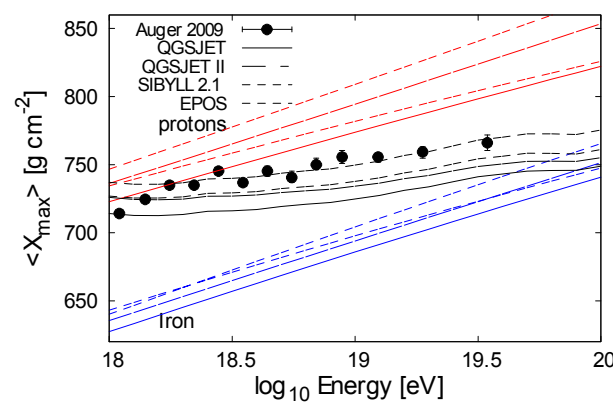
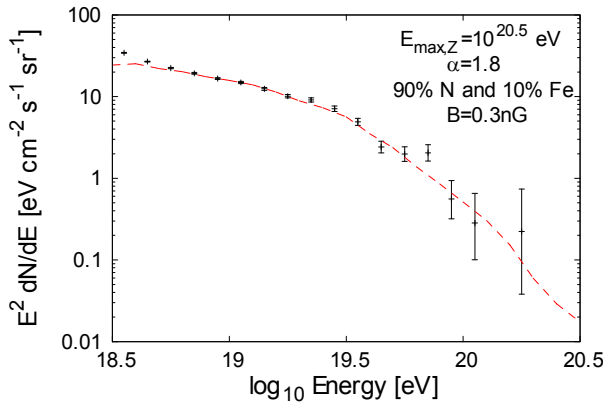
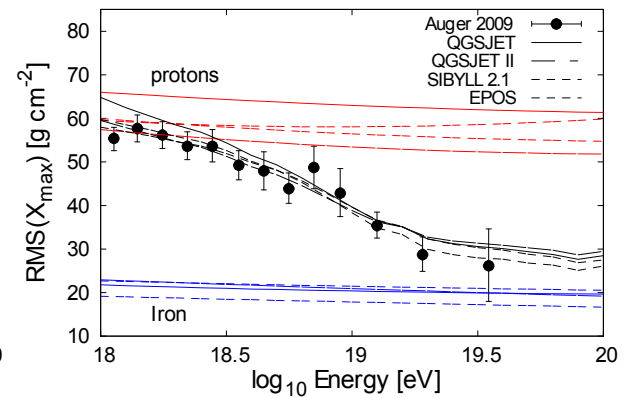
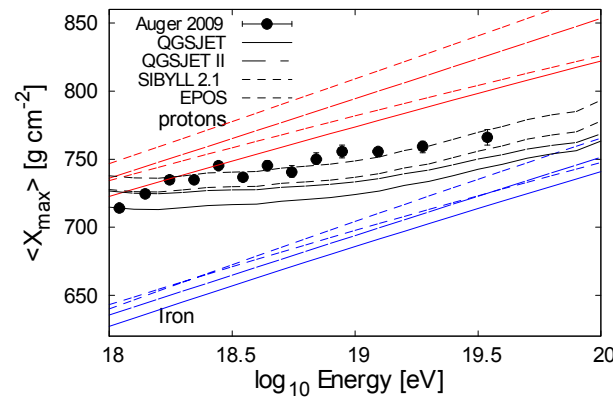
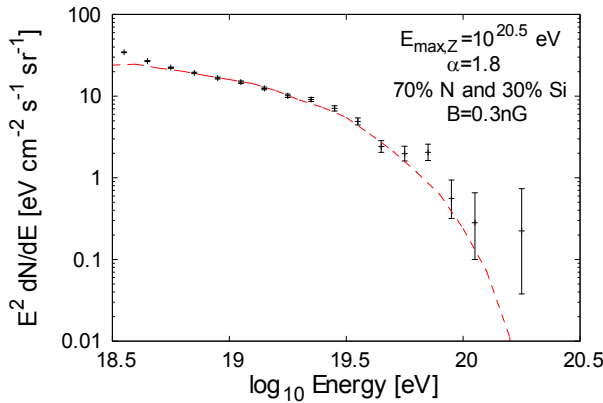
Spectrum and composition fitting

90% N and 10% Fe

70% N and 30% Si

$$B = 0.3nG, L_{cor} = 1Mpc$$

Dan Hooper et al. astro-ph: 0910.1842v1



Conclusions

- Auger spectrum can not be fitted with homogeneously distributed pure proton source
- Fitting $\langle X_{\max} \rangle$ & $\text{RMS}(X_{\max})$ along with spectrum shape strongly constrain possible models of cosmic ray sources
- UHECR source distribution effects may be important

Magnetic field observational limits

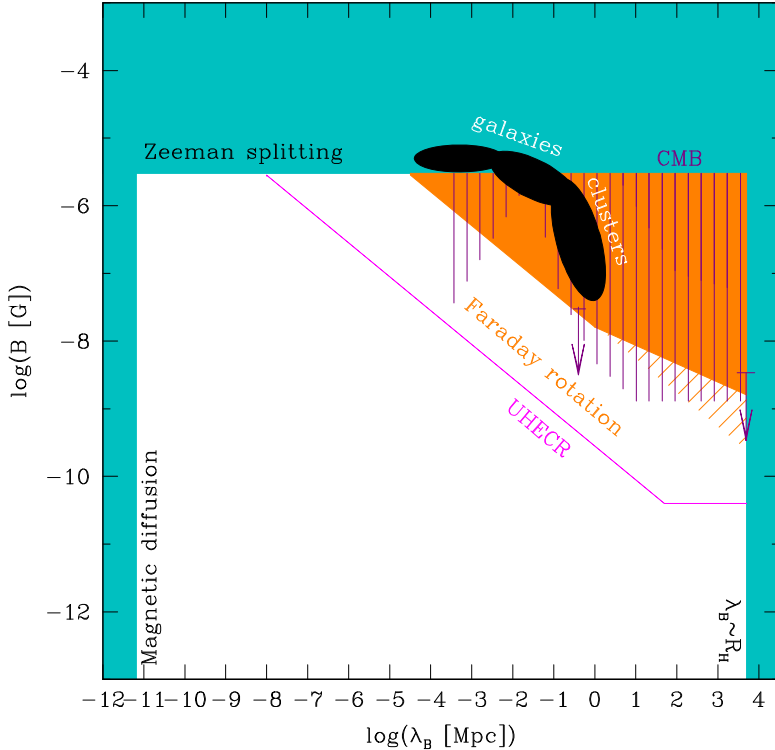


FIG. 1: Observational limits on EGMF. Cyan shaded region shows the upper limit on B imposed by the Zeeman splitting measurement, the lower bound on the correlation length imposed by the magnetic diffusion and the upper bound on correlation length given by the Hubble radius. Orange shaded region shows the limit from Faraday rotation measurements. Filled orange region shows the limit derived in the Ref. [23], while the orange-hatched region is the limit derived in the Ref. [21]. Magenta line shows limit which can be imposed by observations of deflections of UHECR [24]. Violet vertical-hatched regions and the arrows at $\lambda_B \sim 0.5 \text{ Mpc}$ and $\lambda_B \sim R_H$ show the limits imposed on cosmologically produced fields by the CMB observations [36, 37, 40, 45]. Black ellipses show the ranges of measured magnetic fields in galaxies and galaxy clusters.

A. Neronov et al. Phys.Rev.D80:123012,2009

Magnetic field limits

A. Neronov et al. Phys.Rev.D80:123012,2009

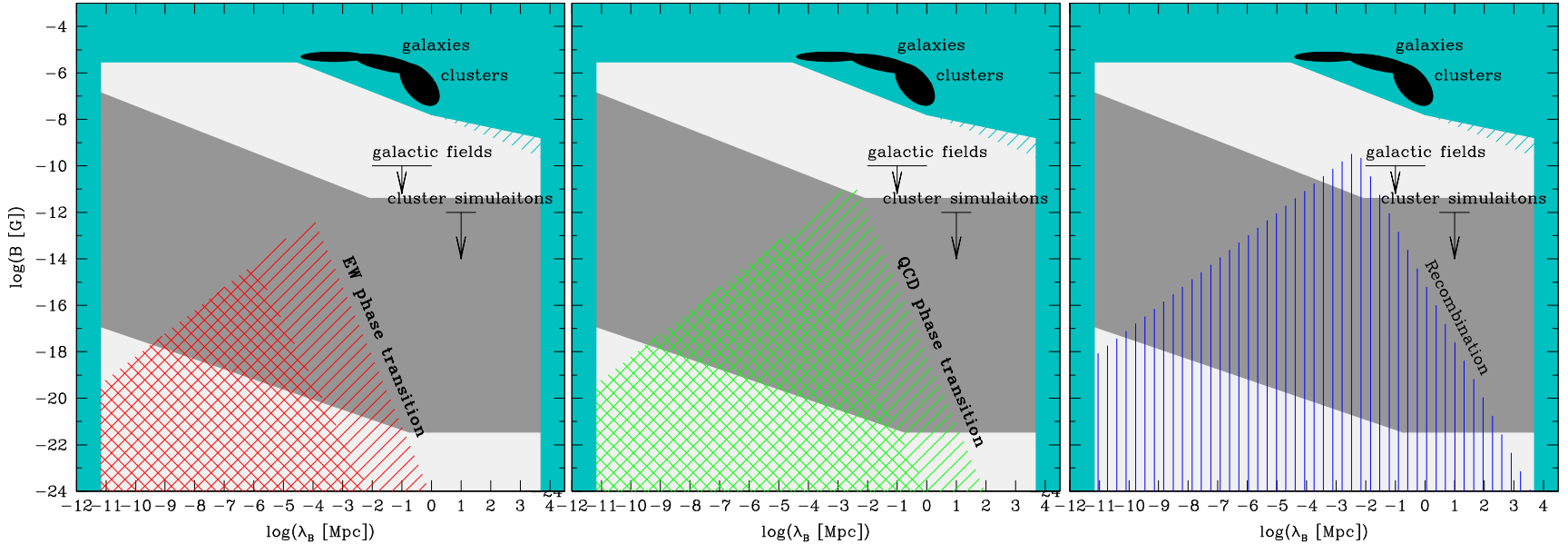


FIG. 2: Model predictions and estimates for the EGMF strength. Cyan shaded region and black ellipses show the experimental limits and measurements from Fig. 2. Upper bound at $B \sim 10^{-10}$ G shown by solid line comes from flux conservation during galaxy formation argument [7]. Upper bound at $B = 10^{-12}$ G shows a limit imposed by constrained simulations of magnetic fields in galaxy clusters [12, 33]. Left panel: left and right hatched regions show theoretically allowed range of values of B, λ_B for non-helical and helical fields generated at the epoch of electroweak phase transition during radiation-dominated era. Middle panel: left and right hatched region show ranges of possible B, λ_B for nonhelical and helical magnetic fields produced during the QCD phase transition. Right panel: hatched region is the range of possible B, λ_B for EGMF generated during recombination epoch. Dark grey shaded region shows the range of (B, λ_B) parameter space accessible for the γ -ray measurements via γ -ray observations. Light-grey shaded regions show the parts of the parameter space in which the existence of EGMF could be confirmed or ruled out, but no measurements of EGMF strength is possible.